Journal of Solid State Chemistry **160,** 212–221 (2001)
doi:10.1006/jssc.2001.9225, available online at http://www.idealibrary.com on IDEAL®

Some Factors Governing Ag^+ and Cu^+ Low Coordination in Chalcogenide Environments

Etienne Gaudin, Florent Boucher,[1] and Michel Evain

Laboratoire de Chimie des Solides, I.M.N., UMR C6502 CNRS - Université de Nantes, 2 rue de la Houssinière, BP 32229, 44322 Nantes Cedex 3, France

Received March 15, 2001; accepted April 20, 2001; published online June 7, 2001

The factors influencing the low coordination of Cu^+ and Ag^+ d^{10} cations in chalcogenides are analyzed by means of FLAPW band structure calculations. The study shows that the metal *s*/*d* orbital mixing is the predominant factor, in agreement with most previous research reports. It also quantitatively shows that the d^{10} cation polarization is reduced when the chalcogen electronegativity decreases, thus the coordination increases when going from the oxides to the tellurides. The calculation results make clear the fact that the d^{10} element low coordination can be raised for a given chalcogen by enhancing the polarization influence of the chalcogen through a charge transfer from an alkali metal. Finally, the shift in behavior from Cu^+ to Ag^+ is shown to be related to their different polarizabilities. © 2001 Academic Press

Key Words: **chalcogenides; d^{10} cation; silver and copper coordination; band structure calculations; FLAPW.**

1. INTRODUCTION

Particular attention has been paid to d^{10} cations such as Ag^+ and Cu^+ because of their specific properties and especially their stability in low coordination environments. With filled *d*-electron shells, those ions could be at first sight considered as stereochemically equivalent to, say, alkali or alkaline earth ions, which in fact is not the case. As early as 1958, Orgel (1) suggested that the low coordination (twofold, threefold, or fourfold) they usually adopt, opposite to ionic crystal structure simple theory predictions, was due to a hybridization of the metal filled *d* orbitals with the metal empty *s* orbitals (*M d*/*s* hybridization). For such a hybridization to occur, the *d*–*s* energy separation should not be too large. Thus the expected tetrahedral or octahedral environment is observed for Zn^{2+} and Cd^{2+}, for which the energy separation is rather large (2). Extensive calculations (3–5) have been performed on Cu_2O. They confirm the deviation from an ionic model and the importance of the *M d*/*s* hybridization. This explanation of the low coordination stability of Ag^+ and Cu^+ has been the description prevailing in some general inorganic chemistry books (6, 7). It has been further developed by Burdett and Eisenstein (8) who showed that the distortion from regular tetrahedral or octahedral environment resulted from a second-order Jahn–Teller effect.

A totally different interpretation of the low coordination stability of Ag^+ and Cu^+ was given by Tossell and Vaughan (9), on the basis of spectra and molecular calculations and XPS and XES assignments. Their analysis indicates that the major factors driving the low coordination stability are the metal *d*- ligand *p* (*M d*–*L p*) energy separation and the extent of the *M d*–*L p* orbital mixing. Considering the following two points: (i) the splitting between bonding and antibonding levels is proportional to the square of the orbital overlap and is inversely proportional to the difference in energy between the atomic orbital levels and (ii) a high coordination tends to raise the *M d* level energies as compared to the *L p* level energies, they explain the coordination of some cations, and specifically that of Ag^+ and Cu^+. Indeed, the cations avoid low coordinations if the *M d* orbitals are higher in energy than the *L p* orbitals and the energy gap is not too large since a low coordination would imply a lowering of the *M d* level and an increased *M d*–*L p* interaction that would destabilize the filled antibonding *M d* levels. They prefer low coordinations in the opposite case (i.e., *M d* levels below *L p* levels) to maximize the *M d*–*L p* energy gap and achieve a lowering of the filled antibonding *M d* levels. In Fig. 1, the relative level positions for copper and silver in oxides and sulfides are shown, as depicted by Tossell and Vaughan in (9). For the copper compounds, the *M d* levels are above the *Mp* levels of oxygen and sulfur anions. The Cu *d*–O *p* energy difference is too large to oppose a linear coordination, thus the linear coordination in Cu_2O. In contrast, the Cu *d*–*S p* energy difference is small and will drive a higher coordination as confirmed by the approximate threefold coordination of Cu in Cu_2S. Following the same arguments, in silver chalcogenides a linear coordination is expected for silver ions with both oxygen and sulfur anions; this is indeed the case in Ag_2O and Ag_2S (although

[1]To whom correspondence should be addressed. E-mail: Florent. Boucher@cnrs-imn.fr

0022-4596/01 $35.00

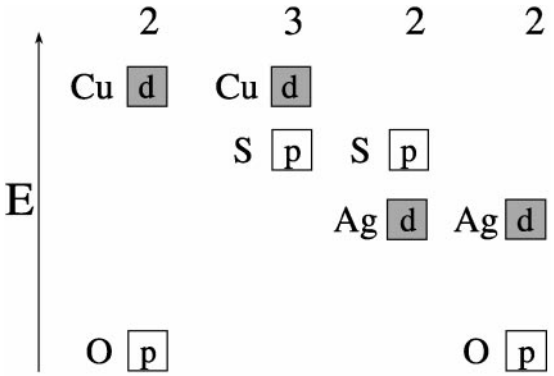

FIG. 1. Relative metal *d* versus anion *p* level positions for copper, silver, oxygen and sulfur in binary chalcogenides (9).

both linear and triangular coordination are observed in Ag_2S).

The model originally proposed by Orgel and subsequently developed by further studies highlighted a reason for the low coordination of Cu^+ and Ag^+ but did not explain the coordination change implied by a covalence modification. For instance, why is copper triangularly coordinated in Cu_2S but only linearly coordinated in KCuS? Similarly, why does copper coordination evolve from 2 in Cu_2O to 3 in Cu_2S and Cu_2Se? In contrast, Tossel and Vaughan focussed on the coordination preference as a function of the ligand choice but did not take into consideration the *M s/d* hybridization. To pinpoint the actual factors governing the stabilization of the Cu^+ and Ag^+ d^{10} cations in chalcogenides, we initiated band structure calculations by means of the full-potential linearized augmented plane waves (FLAPW) method. Several test compounds were chosen for the analysis: basic binary (Cu_2O and Ag_2O) or ternary (AgCuS) chalcogenides, along with an additional series of alkali substituted compounds (KCu*X*, X = O, S, Se, and Te) since a coordination change may be induced through a partial Cu → alkali metal substitution or a chalcogen change.

2. CALCULATION APPROACH

The self-consistent band structure calculations were carried out using a scalar relativistic version of the full-potential linearized augmented plane waves (FLAPW) method, as embodied in the WIEN97 code (10). The exchange and correlation effects were treated within the density functional theory (DFT) using the generalized gradient approximation (GGA) suggested by Perdew *et al*., (11). In the FLAPW method, the unit cell is divided into two parts: nonoverlapping atomic spheres and interstitial regions. Inside the atomic spheres the basis set is a linear combination of atomic-like wave functions. Both the core and valence states are calculated self-consistently: the core states fully relativistically in a spherical atomic approximation and the valence states using the full potential. The local orbital extension (12) is used to treat accurately both the semi-core states (K 3*s*3*p*; Cu 3*p*; Ag 4*p*; O 2*s*; S 3*s*; Se 3*d*4*s*; Te 4*d*5*s*) and the valence bands. The *l* expansion was taken up to $l = 10$. For a better chemical interpretation, the final set of atomic radii were chosen according to the partitioning of the valence electronic density. They are given for each calculation in Ref. (13). In the interstitial region, plane waves (PW) are used with a cut-off parameter $R_{min}{*}K_{max} = 8.0$, where R_{min} is the smallest sphere radius and K_{max} is the maximum wave vector value for the PW. The Brillouin-zone (BZ) integration was performed with a modified tetrahedron method (14). The number of PW and irreducible *k* points used for the calculations are reported in Ref. (13).

3. Cu_2O AND KCuO

Since Cu is found in a linear coordination of oxygen in Cu_2O (15) as well as KCuO (16) (see Fig. 2), an analysis of

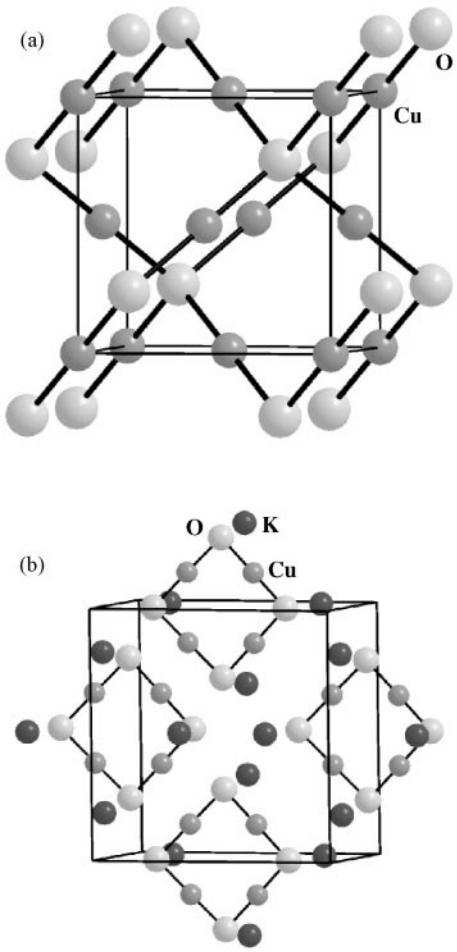

FIG. 2. (a) Cu_2O structure (15) with two interpenetrating networks of copper. Copper ions in linear coordination. (b) KCuO structure (16) exhibiting planar Cu_4O_4 entities separated by isolated potassium cations. Copper ions in linear coordination.

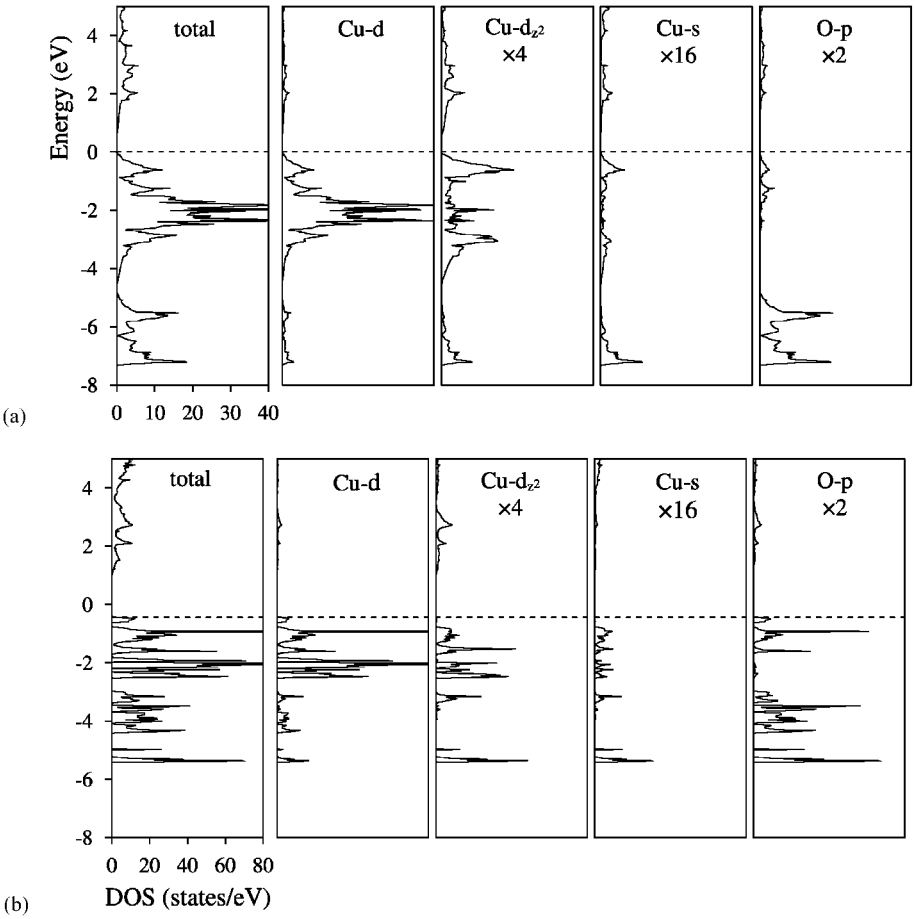

FIG. 3. Total DOS and projected DOS calculated for (a) Cu_2O and (b) KCuO.

the electronic structures calculated for both compounds should emphasize the electronic changes induced by the partial substitution of copper metal atoms by potassium alkali metal atoms.

Cu_2O

The total density of state (DOS) for Cu_2O is presented in Fig. 3a, along with the major band characters extracted from projected DOS. The energy reference is defined according to Ref. (13). The low-lying band (not shown in Fig. 3a) is coming mainly from the O *s* states. The next band, O *p* in character, is slightly overlapping the Cu *d* band. This calculated DOS is perfectly in agreement with Marksteiner *et al.* LAPW calculations (3). It is worth noticing that the major Cu–O interaction occurs between the Cu 4*s* and O 2*p* orbitals because of a large wave function overlapping. This important fact, which has been very well described by Folmer (17), is often neglected in discussing the band structure of transition metal compounds. As a consequence, some of the primarily Cu *s* bands are pushed up in energy. Simultaneously, the Cu–O covalent bonding is achieved through the mixing of the Cu *s* orbitals with some O *p* orbitals, which lowers the latter levels and explains the splitting of the O *p* band. Looking at the partial DOS (Fig. 3a), the Cu *s* contribution to the O *p* block seems very weak, but its real magnitude should in fact be significant. Indeed, the calculation of the partial DOS considerably reduces the apparent Cu *s* contribution. Indeed the fraction of the diffuse 4*s* function which is outside the copper spheres cannot be taken into account in the DOS calculation, as already pointed out by Marksteiner *et al.* (3).

The second interaction to be considered is the *M d–L p* interaction. Because of the smaller expansion of the *d* orbitals, this interaction is weaker than the *M s–L p* interaction we have just described. In general, the *M d–L p* energy separation is too large for the interaction to be significant. However, in copper or silver chalcogenides, the gap in energy is rather small and the interaction may be important (17). In the case of filled *M d* orbitals above the *L p* block, the *M d–L p* interaction lowers the *L p* orbitals and then reduces the *M s–L p* main interaction. The reverse takes place when the *M d* orbitals are below the *L p* block. In Cu_2O, the Cu–3*d* orbitals are above the O–2*p* levels and the interaction reduces the Cu 4*s*–O 2*p* main interaction.

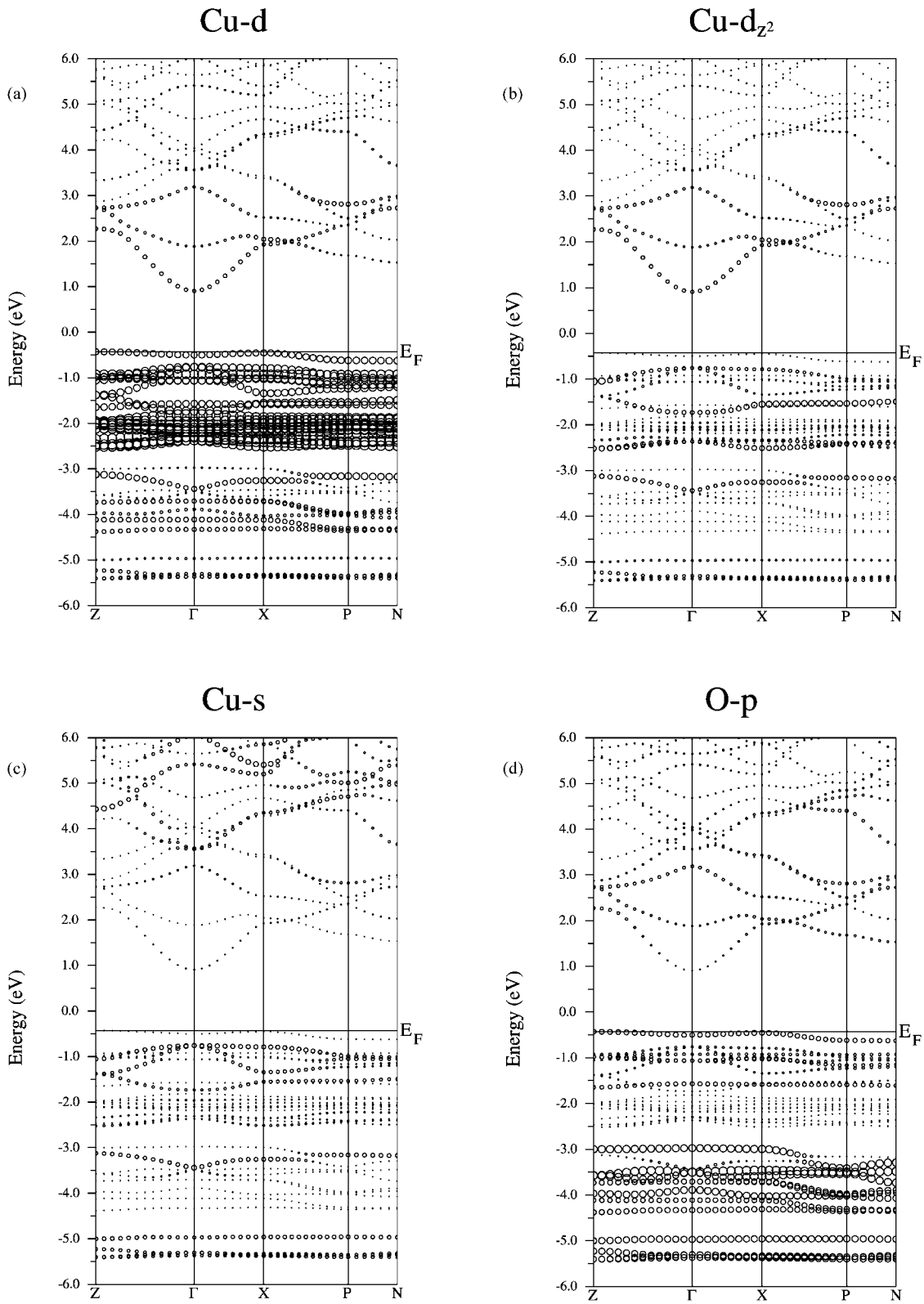

FIG. 4. Energy dispersion curves for KCuO, where $\Gamma = (0, 0, 0)$, $X = (\frac{1}{2}, \frac{1}{2}, 0)$, $P = (\frac{1}{2}, \frac{1}{2}, \frac{1}{2})$, $N = (\frac{1}{2}, 0, \frac{1}{2})$, $Z = (1, 0, 0)$. The various orbital contributions are visualized as "fat band" representation, that is, with a band enlargement proportional to the atomic contribution.

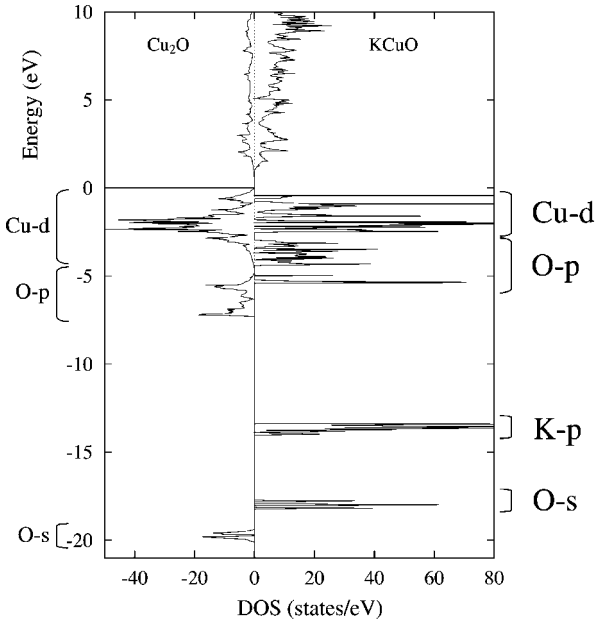

FIG. 5. Total DOS calculated for Cu_2O and KCuO with the same energy scale showing the raising in energy of the O *s* and *p* bands for KCuO.

Finally, let us consider the $M\,s/d$ hybridization. This hybridization and more specifically the $M\,s/d_{z2}$ hybridization is clearly seen in Fig. 3a (Cu d_{z2} contribution in the Cu 4*s* block and vice versa). Notice that the *z* axis of the local coordinate system points toward the nearest oxygen neighbor. A perfect matching of the d_{z2} and *s* partial DOS is also observed in the most bonding part of the O *p* band, at the bottom and at the top of the Cu *d* band and, finally, at the bottom of the conduction band. This is in perfect agreement with the Orgel's model (1). The concept of the $M\,s/d$ hybridization is also supported by Marksteiner *et al.* (3) and experimental proofs have recently been given (5, 15). A schematic view of the various Cu–O interactions is presented in I.

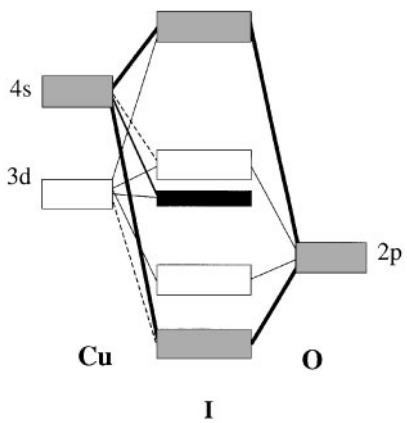

I

TABLE 1
Partial Charge in Electron per Copper Atomic Sphere in Cu_2O and KCuO

	Total	*s*	*p*	*d*	d_{z2}	d_{xz} d_{yz}	d_{xy} d_{x2-y2}
Cu_2O	14.59	0.14	6.01	8.43	1.47	1.76	1.72
KCuO	14.59	0.165	6.02	8.40	1.43	1.76	1.72

Note. For the symmetry analysis, the *z* axis is chosen along the Cu–O bond.

KCuO

The introduction of potassium atoms in the composition to form KCuO isolates the Cu–O chains (see Fig. 2b) and induces an overall increase of the structure ionicity. This is clearly demonstrated by sharper peaks in the DOS (Fig. 3b versus Fig. 3a). In Fig. 4, the energy dispersion curves for KCuO are presented, along with the various orbital contributions emphasized as fat bands (bands enlarged as a function of the atomic contribution). The different interactions described in I for Cu_2O are also observed in KCuO.

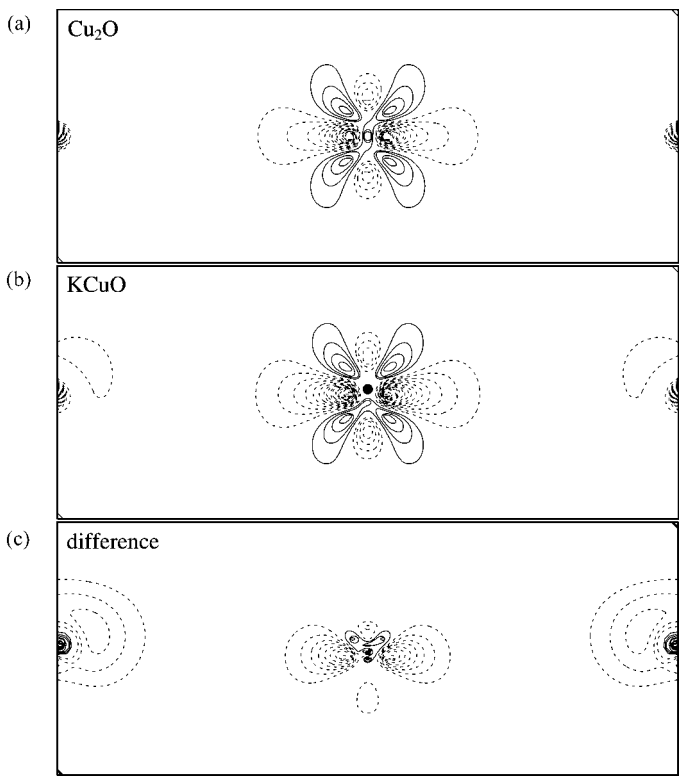

FIG. 6. Contour maps of the difference charge density (see text) for (a) Cu_2O and (b) KCuO. Contour increments of 0.25 $e^-/Å^3$ and -0.25 $e^-/Å^3$ for positive (continuous line) and negative contours (dashed line), respectively; (c) difference contour map between the maps (a) and (b) with contour increments of 0.125 and -0.125 $e^-/Å^3$.

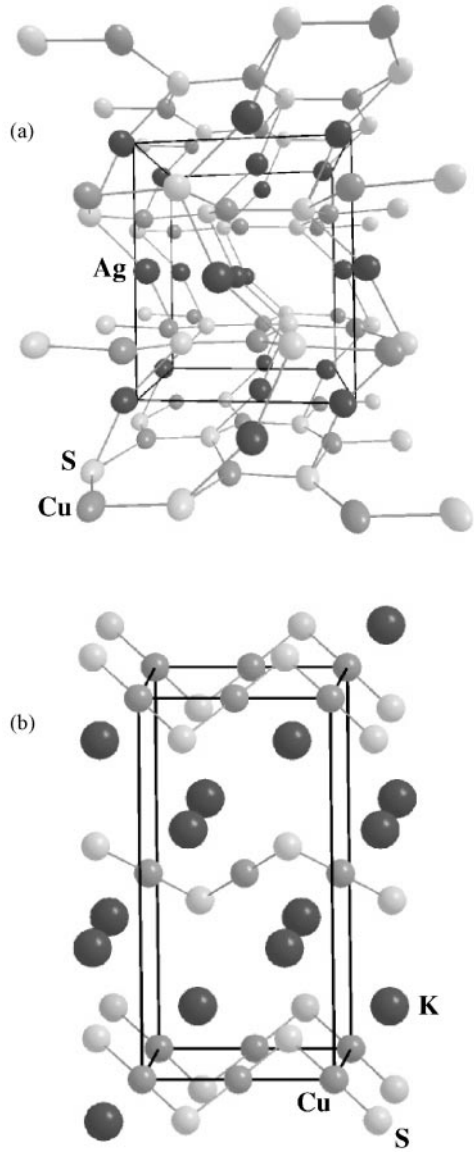

FIG. 7. (a) AgCuS structure (21) with copper in triangular coordination and silver in linear coordination. (b) KCuS structure (20) with chains of copper in linear coordination separated by isolated potassium cations.

The stabilization of some bands at the bottom of the O–*p* block is easily identified as the σ Cu *s*– O *p* bonding interaction (Figs. 4c and 4d) and the important lowering of one Cu *d* band which slightly overlaps the O *p* block correspond to the $M\,s/d_{z^2}$ hybridization (Figs. 4b and 4c). The $M\,s/d_{z^2}$ hybridization also appears in the σ Cu *s*– O *p* bonding block. As expected, the lower part of the Cu *d* block is nonbonding with respect to the Cu *d*– O *p* interaction, and the upper part of the Cu *d* block is antibonding.

The partial substitution of copper by potassium from Cu_2O to KCuO increases the charge density at the oxygen anionic site, with the largest contribution being expected from the potassium atoms. Accordingly, it raises the O *s* and *p* bands, a clear trend is observed in Fig. 5. As a consequence, the Cu–O bond covalence is increased and a higher contribution of the Cu *s* orbitals in the O *p* block is expected. One could quantify this Cu–O covalence increase by comparing the WS partial charges as carried out by Burdett *et al.* in their oxidation state stability analysis (18). This may be, however, hazardous since the partial charge within the WS spheres is highly dependant on the sphere size, that is, the orbital character increases with the sphere size. In our study, a quantitative comparison is nevertheless possible since we have used identical copper atomic spheres in Cu_2O and in KCuO and we have defined the atomic sphere radii from the partitioning of the valence charge density. A summary of the partial charges thus calculated is given in Table 1. We notice that Cu *s* partial charge is larger in KCuO than in Cu_2O, which is a confirmation of the higher Cu–O covalence already envisioned from the band displacements. The change in the Cu–O covalence is also visible in the Cu *d*– O *p* interaction. Indeed, as already pointed out by Marksteiner *et al.* (3), the population of the Cu d_{z^2} orbital in Cu_2O is about 15% smaller than the population of the other Cu *d* orbitals, a phenomenon that has been called a "*d* hole." Recently Zuo *et al.* have experimentally evidenced the existence of this *d* hole (5). The *d* hole corresponds to the fraction of the antibonding Cu *d*– O *p* contribution to the DOS which is pushed above the Fermi level, a consequence of both the Cu s/d_{z^2} hybridization and the interaction between the Cu *d* and the O *p* orbitals. The stronger the covalence of the *M*–*L* interaction, the larger the importance of the *d* hole. In KCuO there is a decrease of the d_{z^2} partial charge, as compared to the CuO case, thus indicating a larger covalence of the Cu–O bonds.

Comparison of the Cu_2O and KCuO Crystal Charge Densities

A very useful method to study the charge transfer and the covalence is the comparison between the crystal charge density and the charge density of superposed free atoms. The advantage of this method is that the obtained information does not depend upon the basis. Several examples of such analysis have already been given for Cu_2O: see for instance Marksteiner *et al.* (3), Ruiz *et al.* (4), or Zuo *et al.* (5).

A contour map of the calculated density difference map (ddm) is given in Fig. 6 for (a) Cu_2O and (b) KCuO, in a plane containing the O–Cu–O axis and the Cu $3d^9 4s^2$ and O $2s^2 2p^4$ spherical configurations being taken as references (notice that the usual Cu $3d^{10} 4s^1$ atomic configuration could not be used in WIEN97 because of computational instabilities). As expected from the previous discussion the difference density around the copper atom is not spherical and its shape can be interpreted on the basis of a simple molecular orbital scheme. The positive contour levels correspond to nonbonding Cu *d* orbitals which have a larger

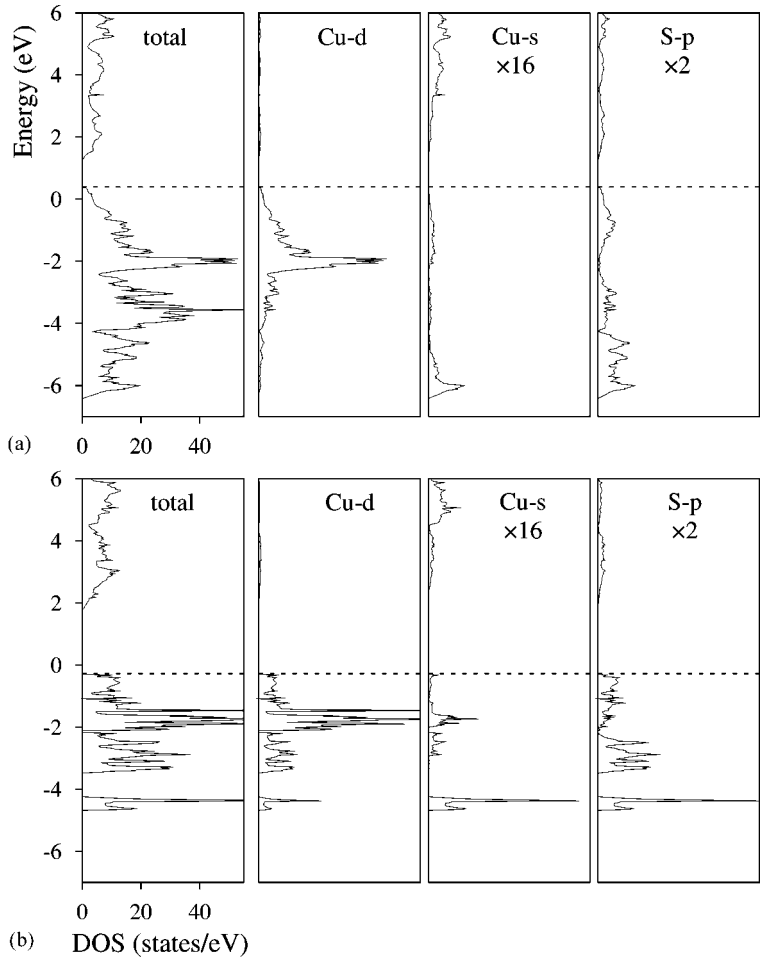

FIG. 8. Total DOS and projected DOS calculated for (a) AgCuS and (b) KCuS.

population than in the spherical configuration. In contrast, the negative contour levels correspond to Cu orbitals with a smaller electronic population than in the spherical configuration, therefore to the *d* hole. The latter orbital can easily be identified as the Cu d_{z2} bonding orbital. The bottom part of Fig. 6 presents the difference between the KCuO and Cu_2O difference density maps (ddm(KCuO)–ddm(Cu_2O)). It perfectly illustrates the smaller population of the d_{z2} orbital in KCuO and thus backs up our covalence arguments.

Another possibility to justify the stronger deformation of the electronic density around Cu in KCuO is to consider the polarization effect of the anions on the quadrupolar polarizability of the copper cations. The polarization influence of the cations is effectively stronger in KCuO because of an increase of the effective charge on the oxygen ions. Such an argument will be fully developed later on in the discussion.

4. AgCuS AND KCuS

In the low temperature form of Cu_2S (19), copper is found in close-to-triangular sites. When half the copper atoms are substituted by potassium atoms, that is, in KCuS (20), the copper coordination is lowered to a linear arrangement. The analysis of the electronic changes induced by the alkali metal should therefore give some insights on the d^{10} low coordination stability. Unfortunately, the cell of Cu_2S is at the moment much too large to allow easy FLAPW calculations. Fortunately, the AgCuS low temperature polymorph (21) also derives from the Cu_2S high temperature structure (22) and the AgCuS unit cell is much smaller and exhibits copper atoms in threefold coordination only, the silver atoms occupying the linear ones (see Fig. 7 for Cu_2S and AgCuS low temperature structures). It has then been assumed that the Cu atoms in AgCuS could mimic those in Cu_2S, as far as their properties were concerned, and band structure calculations were consequently carried out on AgCuS and KCuS.

In Fig. 8, the total and the partial DOS for AgCuS and KCuS are presented. The evolutions that were identified between the Cu_2O and KCuO band structures are also detected when going from AgCuS to KCuS. Indeed, the rise in energy of the anionic levels and the increase of the ionic

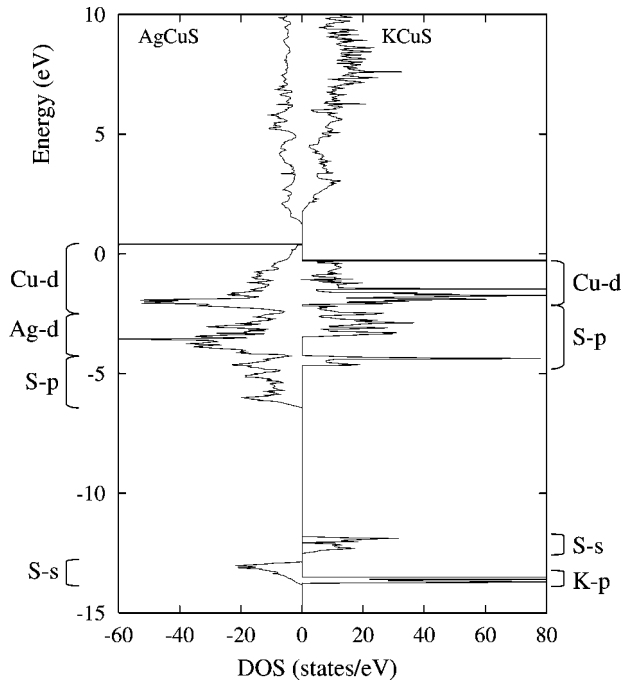

FIG. 9. Total DOS calculated for AgCuS and KCuS showing the raising in energy of the S *s* and *p* bands for KCuS.

character of the structure are both observed (see also the comparison of the total DOS on the same energy scale in Fig. 9). In addition, the quantification of the alkali metal effect on the contribution of the copper 4*s* crystal orbitals to the primarily 3*p* levels of sulfur also reveals an increase of the Cu–S covalence in KCuS, as reflected by the intensification of the partial charge imputed to the Cu *s* orbitals (see Table 2). Our proposed interpretation for the Cu_2O/KCuO system is thus confirmed. Notice that the effect of the alkali metal on the mixing of the Cu *d*–S *p* crystal orbitals is not

TABLE 2
Partial Charge in Electron per Copper Atomic Sphere in AgCuS and KCuS

	Total	*s*	*p*	*d*
AgCuS	14.90	0.17	6.08	8.65
KCuS	14.92	0.21	6.07	8.635

easily detected and only a very small decrease of the Cu *d* population is observed in Table 2. The covalence increase is only clearly seen in the indirectly linked Cu *s*–Cu *d* hybridization expansion. Thus, the Cu *d*–S *p* mixing (the only interaction considered by Tossel and Vaughan) probably contributes to the d^{10} element low coordination stability but is not the predominant factor.

5. KCuO, KCuS, KCuSe, AND KCuTe

As we go down the chalcogen column from oxygen to tellurium, the Cu *d*–*X* *p* energy difference is reduced as revealed by the band energy positions presented in Fig. 10. This covalence increase is to be correlated to a change of coordination from 2 for KCuO (16) and KCuS (20) to 3 for KCuSe (23) and KCuTe (23). However, this behavior is opposite to what is usually expected, that is an increase of the coordination number with a decrease of the covalent character of the bond (24). Therefore, a particular mechanism must be sought.

Although Marksteiner *et al.* in their study on Cu_2O (3) consider the Cu *s*/*d* hybridization as a covalent contribution instead of a polarization, the following research works (25, 26) converge to the conclusion that the quadrupolar polarizability of the Cu^+ and Ag^+ d^{10} cations involved in

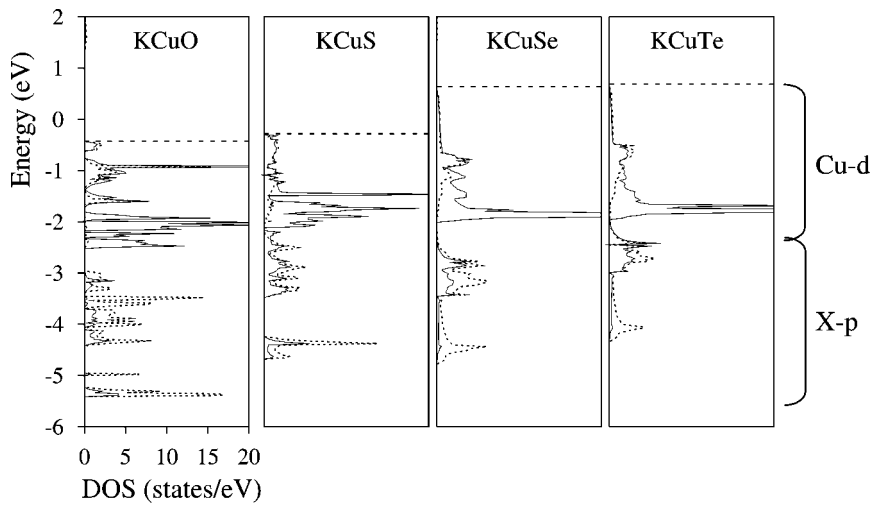

FIG. 10. Partial DOS calculated for the KCu*X* series (*X* = O, S, Se, Te) with Cu–*d* and *X*–*p* contributions in continuous and dashed line, respectively. Copper is in linear coordination in KCuO and KCuS and in triangular coordination in KCuSe and KCuTe.

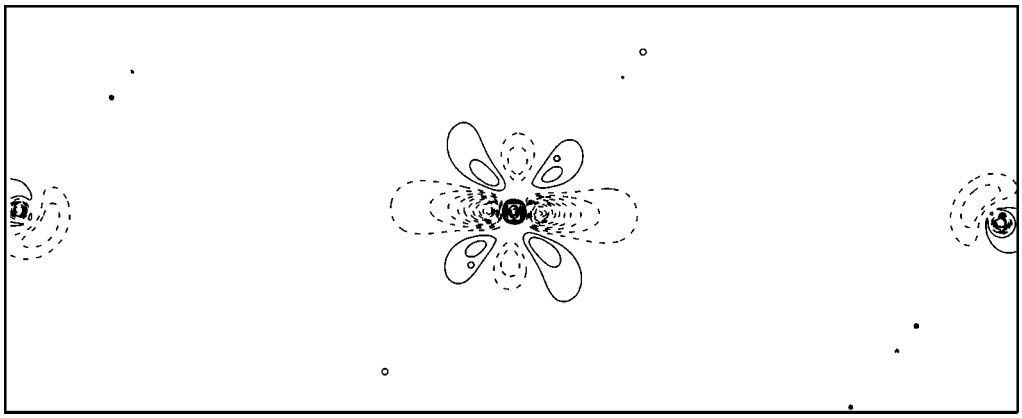

FIG. 11. Contour maps of the difference charge density (see text) for KCuS. Contour increments of $0.25\,e^-/Å^3$ and $-0.25\,e^-/Å^3$ for positive (continuous line) and negative contours (dashed line), respectively.

the $M\,s/d$ hybridization is the most important factor in stabilizing their observed low coordination. Cations such as Cu^+ and Ag^+ (charge density of 177 and 72 C/mm^3, respectively, for a coordination number of 2) are polarizing cations, even toward O^{2-} (charge density of 43 C/mm^3 for a coordination number of 2), because of the poor screening of their d electrons. Nevertheless, they can themselves be polarized as shown by their s/d mixing. Going down the chalcogenide column, the polarizing influence of the chalcogen is considerably reduced with a density charge going from 43 (O) to 8.6 C/mm^3 (Te). The coordination change in copper chalcogenides from 2 in Cu_2O to 3 in Cu_2S can than be understood as a polarization reduction, the lower the d^{10} cation polarization the less stable the low coordination. As an example, in KCuS the polarizing power of the sulfur ion is increased compared to the situation in Cu_2S, and the linear coordination is preferred. A difference density map around copper in KCuS is given in Fig. 11. The polarization of the d electron cloud is effectively visible with a depletion corresponding to the d_{z2} hole. However, the deformation is smaller than in KCuO (Fig. 6) because of the smaller polarizing influence of sulfur.

6. Ag_2O AND AgCuS (Ag_2S)

Following the previous discussion, the polarization of Ag^+ is expected to be smaller in Ag_2S than in Ag_2O because of the decrease of the chalcogen polarizing influence. The structure of Ag_2O (27) is similar to that of Cu_2O (see Fig. 2) with silver atoms in perfect linear coordination. Since the Ag_2S structure is not accurately determined (powder diffraction study with $R = 0.168$) (28), we preferred to consider AgCuS (single crystal study, $R = 0.036$) (21) for the analysis of the chalcogen influence. Notice that the silver atom surrounding in AgCuS is very close to the surrounding observed in Ag_2S with, in both cases, silver in a slightly distorted linear site ($\langle$S–Ag–S$\rangle = 159°$ and 157° and $\langle$Ag–S$\rangle = 2.48$ and 2.49 Å in AgCuS and Ag_2S, respectively).

The comparison of the difference density maps (between the crystal charge density and the charge density of superposed spherical atoms) around the silver atoms for Ag_2O and AgCuS (Fig. 12) clearly shows the reduction of the d orbital deformation when going from the oxide to the sulfide, as previously observed for copper from KCuO to KCuS. Notice that the difference charge densities seem smaller for silver than for copper although silver atoms are

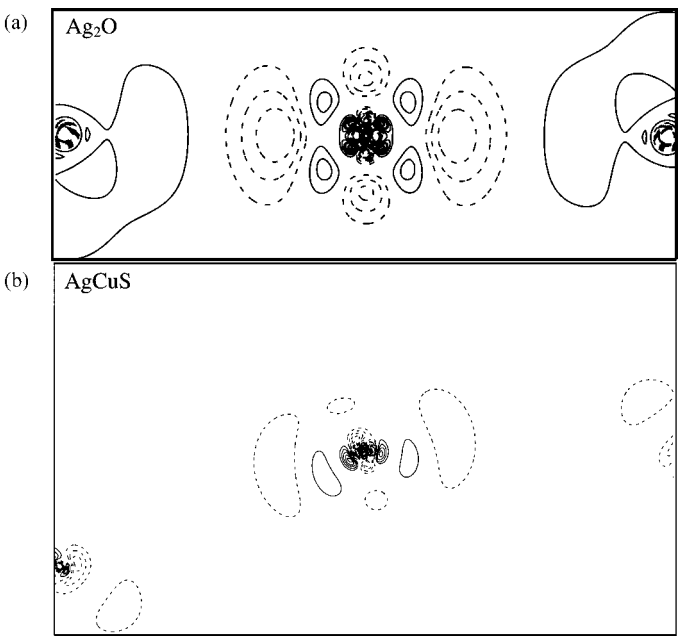

FIG. 12. Contour maps of the difference charge density (see text) for (a) Ag_2O and (b) AgCuS. Contour increments of $0.1\ e^-/Å^3$ and $-0.1\ e^-/Å^3$ for positive (continuous line) and negative contours (dashed line), respectively.

more polarizable than copper atoms. In the case of AgCuS, the silver *d* orbital deformation is even difficult to observe. This should be related to the more diffuse character of the Ag *d* orbitals and the large spread in space of the densities. An integration of that density, if possible, should be more revealing. Finally, it is worth noticing that the Ag *d* orbitals have been found bellow the Cu *d* orbitals (in agreement with the second ionization energies of Ag and Cu, 2073 and 1958 kJ/mol, respectively) but above the S *p* orbitals (see Fig. 9), that is in contradiction with the results of the MS–$X\alpha$ calculations carried out by Tossel and Waughan on Ag_2S (see Fig. 1).

7. CONCLUSION

The $M\,s/d$ mixing is the predominant factor in stabilizing d^{10} Cu^+ or Ag^+ in low coordination environments. In copper chalcogenides, the d^{10} cation polarization is reduced when going from the oxides to the sulfides, then the linear coordination in Cu_2O and the triangular coordination in Cu_2S and Cu_2Se. An increase of the polarization influence of the chalcogen anion can be achieved through a charge transfer resulting from a partial substitution of copper atoms by alkali metals, as observed in KCuS. A coordination change from 2 to 3 is thus observed when going from KCuS to KCuSe, two compounds with two initially less polarizing ligands. This goes against Tossel and Vaughan's model in which a reduction of the $M\,d$–$L\,p$ separation (clearly the case when going from Cu_2S to KCuS) should favor higher coordination (the opposite is observed with a coordination of 3 in Cu_2S and of 2 in KCuS). All the trends that were deduced from the calculations realized on the copper chalcogenides are transferable to the silver chalcogenides (less time consuming LMTO-TB calculations (29) have been performed on Ag_2S and $NaAg_3S_2$ for instance). However, silver being more easily polarized than copper, the coordination change is expected to occur for two heavier chalcogen elements. This is indeed the case since Ag adopts a linear coordination in Ag_2O and Ag_2S (with only one half of the silver atoms in linear sites in the latter compound), but is restrained to triangular sites in Ag_2Se and to tetrahedral sites in Ag_2Te. Once again, the polarizing power of the chalcogen anion can be raised through a charge transfer from a weakly electronegative element and Ag linear sites can be observed in $RbAg_3Se_2$ (30).

REFERENCES

1. L. E. Orgel, *J. Chem. Soc.* 4186–4190 (1958).
2. Jorgensen, thesis, Copenhagen, 1957.
3. P. Marksteiner, P. Blaha, and K. Schwarz, *Z. Phys. B*: *Condens. Matter* **64,** 119–127 (1986).
4. E. Ruiz, S. Alvarez, P. Alemany, and R. A. Evarestov, *Phys. Rev. B* **56,** 7189–7196 (1997).
5. J. M. Zuo, M. Kim, M. O'Keeffe, and J. C. H. Spence, *Nature* **401,** 49–52 (1999).
6. F. A. Cotton and G. Wilkinson, *in* "Advanced Inorganic Chemistry," 5th ed., p. 941. Wiley, Brisbane/New York, 1988.
7. J. E. Huheey, E. A. Keiter, and R. L. Keiter, *in* "Inorganic Chemistry," 4th ed., p. 473. Harper Collins, New York, 1993.
8. J. K. Burdett and O. Eisenstein, *Inorg. Chem.* **31,** 1758–1762 (1992).
9. J. A. Tossel and D. J. Vaughan, *Inorg. Chem.* **20,** 3333–3340 (1981).
10. P. Blaha, K. Schwarz, and J. Luitz, "WIEN97, A full Potential Linearized Augmented Plane Wave Package for Calculating Crystal Properties," Karlheinz Schwarz, Techn. Universität Wien, Austria, 1999.
11. J. P. Perdew, S. Burke, and M. Ernzerhof, *Phys. Rev. Lett.* **77,** 3865–3868 (1996).
12. D. Singh, *Phys. Rev. B* **43,** 6388–6392 (1991).
13. Data used for the band structure calculations on the various compounds are as follows: **Cu_2O:** space group, $Pn\bar{3}m$ (2nd setting); cell parameters, $a = 4.267$ Å; atomic sphere radii (Å) and positions, Cu (0.894// 0, 0, 0), O (0.947// $\frac{1}{4}, \frac{1}{4}, \frac{1}{4}$); 940 Plane Waves (PW) + Local Orbitals (LO); 20 Irreducible *k* Points (IkP). **Ag_2O:** $Pn\bar{3}m$ (2nd setting); $a = 4.76$ Å; Ag (1.111// 0, 0, 0), O (0.947// $\frac{1}{4}, \frac{1}{4}, \frac{1}{4}$); 1093 PW + LO; 20 IkP. **KCuO:** $I\bar{4}m2$; $a = 9.35$ Å, $c = 5.44$ Å; K (0.894// 0.1807, 0, 0.7484), Cu (0.894// 0.3603, 0.8603, $\frac{1}{4}$), O (0.947// 0.7780, 0, 0.2258); 2858 PW + LO; 18 IkP. **KCuS:** $Pna2_1$; $a = 10.66$ Å, $b = 6.20$ Å, $c = 5.32$ Å; K (1.058// 0.6536, 0.0243, 0.749), Cu (0.952// $\frac{1}{2}, \frac{1}{2}, \frac{1}{2}$), S (1.164// 0.5890, 0.2758, 0.255); 3496 PW + LO; 32 IkP. **AgCuS:** $Pmc2_1$; $a = 4.047$ Å, $b = 6.592$ Å, $c = 7.930$ Å; Ag1 (1.217// 0, 0.9440, $\frac{1}{2}$), Ag2 (1.217// $\frac{1}{2}$, 0.4402, 0.9728), Cu1 (0.952// 0, 0.5674, 0.7297), Cu2 (0.952// $\frac{1}{2}$, 0.0663, 0.7424), S1 (1.217// 0, 0.2161, 0.7215), S2 (1.217// $\frac{1}{2}$, 0.7133, 0.7594); 2124 PW + LO; 45 IkP. **KCuSe:** $P6_3/mmc$; $a = 4.18$ Å, $c = 9.54$ Å; K (1.323// 0, 0, 0), Cu (1.106// $\frac{1}{3}, \frac{2}{3}, \frac{3}{4}$), Se (1.302// $\frac{1}{3}, \frac{2}{3}, \frac{1}{4}$); 921 PW + LO; 28 IkP. **KCuTe:** $P6_3/mmc$; $a = 4.46$ Å, $c = 9.95$ Å ; K (1.482// 0, 0, 0), Cu (1.164// $\frac{1}{3}, \frac{2}{3}, \frac{3}{4}$), Te (1.6889// $\frac{1}{3}, \frac{2}{3}, \frac{1}{4}$); 921 PW + LO; 28 IkP. For the comparison of the density of states, an absolute energy scale has been defined. The Fermi level of Cu_2O is used as the zero energy level. Then, for a given chalcogenide, the energy position of the 1*s*(Cu) core state is taken as a constant and from one chalcogenide to another the energy position of the 1*s*(K) core state is used as a reference: 1*s*(Cu) at -8842.961 eV for Cu_2O and KCuO and 1*s*(K) at -3514.922 eV for KCuO, KCuS, KCuSe, KCuTe. One obtains: 1*s*(Cu) at -8842.685 eV for KCuS and AgCuS, -8842.378 eV for KCuSe and -8842.351 eV for KCuTe.
14. P. E. Blöchl, O. Jepsen, and O. K. Andersen, *Phys. Rev. B* **49,** 16,223–16,233 (1994).
15. R. Restori and D. Schwarzenbach, *Acta Crystallogr. Sect. B* **42,** 201–208 (1986).
16. W. Losert and R. Hoppe, *Z. Anorg. Allg. Chem.* **524,** 7–16 (1985).
17. J. C. W. Folmer, thesis, Groningen, 1981.
18. J. K. Burdett and S. Sevov, *J. Am. Chem. Soc.* **117,** 12,788–12,792 (1995).
19. H. T. J. Evans, *Z. Kristallogr.* **150,** 299–320 (1979).
20. G. Savelsberg and H. Schäfer, *Z. Naturforsch. B* **33,** 711–713 (1978).
21. C. L. Baker, F. J. Lincoln, and A. W. S. Johnson, *Acta Crystallogr. Sect. B* **47,** 891–899 (1991).
22. R. J. Cava, F. Reidinger, and B. J. Wuensch, *Solid State Ionics* **5,** 501–504 (1981).
23. G. Savelsberg and H. Schäfer, *Z. Naturforsch. B* **33,** 370–373 (1978).
24. E. Mooser and W. B. Pearson, *Acta Crystallogr.* **12,** 1015–1021 (1959).
25. J. I. McOmber, S. Topiol, M. A. Ratner, and D. F. Shriver, *J. Phys. Chem. Solids* **41,** 447–453 (1980).
26. W. G. Kleppmann and H. Bilz, Comm. *Phys.* **1,** 105–110 (1976).
27. R. W. G. Wyckoff, *Am. J. Sci.* **5,** 184–188 (1922).
28. R. Sadanaga and S. Sueno, *Miner. J. Jpn.* **5,** 124–148 (1967).
29. O. K. Andersen, *Phys. Rev. B* **12,** 3060–3083 (1975); O. K. Andersen and O. Jepsen, *Phys. Rev. Lett.* **53,** 2571–2574 (1984).
30. W. Bronger and H. Schils, *J. Less-Common Met.* **83,** 287–291 (1982).